International Journal of Nanomedicine

Dovepress
Taylor & Francis Group

Open Access Full Text Article

ORIGINAL RESEARCH

Tyrosinase-Responsive Activated Nano-Coated Sensor for Sensitive Detection of Melanoma Biomarkers

Shan Hua[1,2,*], Yun Zha[1,*], Hui Zhou[3,*], Lingling Jia[1,*], Hongyi Zhang[1,2], Jiawei Gu[1,2], Rong Guo[1], Yingshen Shi[1], Hua Jiang[1], Yuxin Qian[1]

[1]Department of Plastic Surgery, Shanghai East Hospital, School of Medicine, Tongji University, Shanghai, 200120, People's Republic of China; [2]Medical College, Tongji University, Shanghai, 200331, People's Republic of China; [3]Department of General Surgery, the second Xiangya Hospital of Central South University, Changsha, 410011, People's Republic of China

*These authors contributed equally to this work

Correspondence: Yuxin Qian; Hua Jiang, Department of Plastic Surgery, Shanghai East Hospital, School of Medicine, Tongji University, Shanghai, 200120, People's Republic of China, Email heliosqyx@163.com; dosjh@126.com

Background: Melanoma is a highly metastatic skin cancer with occult early symptoms, making sensitive diagnostic tools essential for early intervention. Tyrosinase (TYR), a key enzyme in melanogenesis, is aberrantly secreted into the bloodstream by melanoma cells and thus serves as a promising biomarker for melanoma. However, the ultralow concentration of TYR in serum (0.066–0.636 U/L) poses a significant challenge to conventional detection methods, highlighting the need for more sensitive detection strategies.

Methods: An electrochemical biosensor was engineered using a screen-printed electrode (SPE) as the base. The SPE was modified with a nanocomposite consisting of tyramine-functionalized carboxylated multi-walled carbon nanotubes (MWCNTs-tyr), gold nanoparticles (Au NPs), and poly(3,4-ethylenedioxythiophene) (PEDOT). To validate the sensor's performance, differential pulse voltammetry (DPV) was employed, with tests conducted in phosphate-buffered saline (PBS, pH 7.0) and murine serum samples.

Results: The MWCNTs-tyr/Au NPs/PEDOT nanocomposite synergistically enhanced the sensor's conductivity, catalytic activity, and TYR-specific binding capacity. The sensor exhibited a wide linear detection range for TYR (0.05~0.9 U/L, $R^2 = 0.9914$), and a low detection limit of 0.0091 U/L. Additionally, it showed excellent reproducibility (5 consistent measurements at a TYR concentration of 0.1 U/L) and high specificity against common serum interferents. In tumor-bearing mice, TYR serum levels were found to correlate with tumor progression: TYR concentration was 0.084 ± 0.009 U/L when tumor volume was 68 ± 5.25 mm^3, and increased to 0.653 ± 0.028 U/L when tumor volume reached 1280 ± 89.22 mm^3.

Conclusion: This study presents a proof-of-concept for a MWCNTs-tyr/Au/PEDOT/SPE biosensor. The platform enables rapid and sensitive detection of TYR in small-volume samples and effectively monitors tumor burden in a murine model, demonstrating its potential as a research tool for melanoma biomarker investigation.

Keywords: melanoma, tyrosinase, electrochemical biosensor, multi-walled carbon nanotubes, tyramine functionalization, early diagnosis

Introduction

As a highly malignant skin cancer, melanoma is characterized by insidious early symptoms, rapid progression, and a high tendency for distant metastasis, which significantly reduces the 5-year survival rate of patients with advanced disease.[1] Therefore, achieving early diagnosis of melanoma is of crucial clinical significance for improving patient prognosis and enhancing treatment success rates.[2] Among numerous potential diagnostic markers, tyrosinase, as a key rate-limiting enzyme in the process of melanin synthesis, has a close correlation with the occurrence and development of melanoma, and is regarded as a highly promising biomarker for early diagnosis.[3] Under normal physiological conditions, TYR is strictly confined intracellularly within healthy melanocytes and is rarely detectable in the peripheral circulation.

https://doi.org/10.2147/IJN.S565641
Received: 19 September 2025
Accepted: 3 February 2026
Published: 16 February 2026

Graphical Abstract

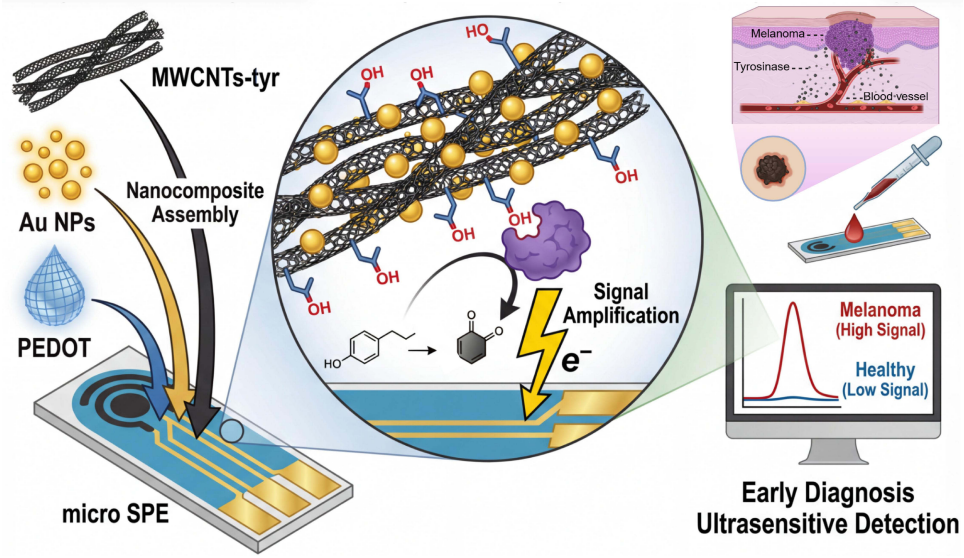

However, in the context of melanoma, the rapid proliferation, high metabolic turnover, and cell lysis of malignant cells lead to the aberrant release and accumulation of TYR into the bloodstream.[4] Although trace levels of TYR activity may theoretically originate from normal skin turnover or other non-malignant pigmented lesions, the serum concentration in melanoma patients is significantly elevated (0.066~0.636 U/L) often orders of magnitude higher than the physiological baseline (≤0.024 U/L). This distinct pathological elevation serves as the biological basis for utilizing circulating TYR as a specific biomarker for melanoma screening and staging.[5,6]

Currently, traditional methods for detecting tyrosinase include enzyme-linked immunosorbent assay (ELISA) and high-performance liquid chromatography (HPLC).[7,8] However, these methods generally have limitations such as cumbersome operation, long detection cycle, reliance on large-scale instruments, and insufficient sensitivity, making them difficult to meet the clinical needs for rapid and accurate early screening of melanoma. In contrast, electrochemical biosensors have shown great application potential in the field of biomarker detection due to their advantages of high sensitivity, rapid response, low cost, and portability, and are particularly suitable for point-of-care testing scenarios in primary medical institutions.[9–11] Among them, screen-printed electrodes (SPEs) have become an ideal platform for portable sensors because of their characteristics of mass production and easy surface modification. The performance of electrode modification materials is the core factor determining the detection performance of electrochemical biosensors.[12,13] However, traditional SPEs have problems such as insufficient conductivity and low interfacial electron transfer efficiency, which limit their ability to detect trace markers.[14]

Multi-walled carbon nanotubes (MWCNTs) have emerged as an ideal candidate for electrode modification due to their excellent electrical conductivity, large specific surface area, and good biocompatibility.[15] Carboxylation modification can endow MWCNTs with more surface active sites, enhancing their water solubility and functionalization potential.[16] Further modification of tyramine is crucial for sensor design. From a biochemical perspective, tyramine is the product of tyrosine decarboxylation and possesses the phenolic structure essential for the tyrosinase active site.[17,18] Unlike other complex substrates, tyramine's primary amine group readily undergoes covalent grafting onto multi-walled carbon nanotubes, while its exposed phenolic group serves as a specific target for tyrosinase-catalyzed ortho-hydroxylation, ultimately yielding electroactive dopamine. This modification not only stabilizes carbon nanotube dispersion through π-π stacking interactions but also enables specific trapping and catalytic recognition by tyrosinase, laying the foundation for subsequent signal transduction.[19] To further improve the electrical conductivity and electrocatalytic activity of the electrode, this study introduces gold (Au) nanoparticles and poly

(3,4-ethylenedioxythiophene) (PEDOT) to prepare a composite nanocoating. Au nanoparticles can accelerate the electron transfer rate and enhance the amplification effect of detection signals.[20] As a conductive polymer with excellent stability, PEDOT:PSS can construct a highly conductive network structure, which is used for immobilizing MWCNTs and Au nanoparticles on the surface of SPEs.[21] Compared with electrode materials prepared by traditional drop-coating and drying methods, this composite coating exhibits higher stability and synergistically enhances the charge transport capability of the composite modification layer.[22] The finally prepared electrode material is expected to significantly improve the sensitivity and specificity of the electrode's electrochemical response to tyrosinase.

Based on the above design concept, this study constructs a novel enzyme-responsive activated biosensor. Distinct from traditional immuno-sensors that rely on steric hindrance or simple adsorption, our strategy utilizes the specific enzymatic conversion of surface-bound tyramine to trigger a turn-on electrochemical signal. This design, integrating the MWCNTs-tyr/Au/PEDOT nanocomposite, not only achieves highly sensitive detection of tyrosinase in melanoma blood samples but also features simple operation and batch reproducibility.

Experimental Section

Materials

All chemicals and reagents were of the highest commercially available grade and were used at the price at the time of receipt. Carboxylated multi-walled carbon nanotubes (WMCNTs-COOH), PEDOT:PSS were purchased from XFNANO (China). $HAuCl_4$, Potassium permanganate, Tyramine, Tyrosinase, Uric acid, Dopamine, L-ascorbic acid, Potassium ferricyanide ($K_4Fe(CN)_6$), Potassium ferricyanide ($K_3Fe(CN)_6$), Potassium chloride (KCl), and uricase were purchased from Sigma-Aldrich (USA).

Apparatus

All electrochemical measurements were performed on a CHI660E (Shanghai Chenhua Instrument Co., Ltd).

Synthesis of Au Nanoparticles

Gold colloids were prepared by bringing 50 mL of an aqueous $HAuCl_4{\cdot}3H2O$ solution (1 mg/mL) to a boil under reflux and stirring (1300 rpm). Subsequently, 5.6 mL of a sodium citrate solution (10 mg/mL) was quickly injected into the boiling precursor. The mixture was refluxed for another 15 min after the appearance of a wine-red color and then cooled to room temperature.

Synthesis of Tyramine-Functionalized MWCNTs (MWCNTs-Tyr)

Disperse 50 mg of MWCNTs-COOH in 50 mL of MES (pH 6.0). Add 200 mg of EDC·HCl and 120 mg of NHS. Stir at room temperature in the dark for 2 hours. Centrifuge (12,000 rpm, 10 min), wash three times with PBS, to obtain MWCNTs-NHS. Resuspend MWCNTs-NHS in 40 mL MES, and react under nitrogen protection at room temperature with shaking for 24 h. Centrifuge (12,000 rpm, 10 min) to remove free tyramine. Wash three times with ultrapure water. Vacuum dry to obtain Tyramine-MWCNTs.

Preparation of MWCNTs-Tyr/Au/PEDOT/SPE Electrodes

Take 5 μL and 3 μL of the above MWCNTs-tyr and Au NPs mixtures, respectively, add 2 μL of PEDOT:PSS, mix evenly, and apply to the SPE electrode. Dry at 37°C.

Characterization

Dynamic light scattering (DLS) measurements were carried out using a Zetasizer Nano-ZS (Malvern, UK) with a standard 633 nm laser at 298.0 K. A JEM-2010 transmission electron microscope (TEM) was used to characterize the morphology of the nanoparticles. High angle annular dark field scanning TEM (HAADF-STEM) images and elemental maps were obtained by Titan Themis 60–300 G2. UV-Vis spectra of different samples were recorded by UV-Vis spectrophotometer Lambda 35 (Perkin-Elmer).

Electrochemical Measurements

All electrochemical measurements were performed on CHI660E with an electrolyte of 0.1 M KCl, 5 mM $[Fe(CN)6]^{3-/4-}$ for Cyclic Voltammetry (CV), Electrochemical Impedance Spectroscopy (EIS) and Differential Pulse Voltammetry (DPV). Differential Pulse Voltammetry (DPV) was employed to monitor the enzymatic reaction product. The measurements were carried out in a potential window from −0.2 V to +0.6 V.

Detection of Tyrosinase

The prepared MWCNTs-tyr/Au/PEDOT/SPE was added with different concentrations of tyrosinase (100 μL) for 30 min. Next, the electrode was washed repeatedly with deionized water to remove unreacted tyrosinase and dried for testing.

Tumor Cells Inoculation

B16F10 cells (ATCC) were cultured with high-glucose Dulbecco's Modified Eagle Medium supplemented with 10% fetal bovine serum (BDBIO) and 1% penicillin-streptomycin (gibco).

B16/F10 cells were cultured to 80% confluence, digested with 0.25% trypsin (New Cell & Molecular Biotech), centrifuged, and resuspended in PBS. BALB/c nude mice (4–5 weeks old) were subcutaneously injected with B16F10 melanoma cells (1×10^6 cells) into the right flank. To monitor the correlation between tumor growth and serum tyrosinase levels, the mice were randomly divided into four groups corresponding to different time points (Day 0, 4, 8, and 12), with a sample size of n = 5 mice per group. Tumor dimensions were measured using a vernier caliper, and volume was calculated as $V = 0.5\times length\times width^2$. At each designated time point, blood samples were collected, and serum analysis was performed in a single-blind manner to minimize bias. A control group injected with 4T1cells (n=5) was established under identical conditions to verify specificity.

Serum Collection and Processing

3% isoflurane inhalation induction, blood collection from the tail vein plexus, using heparinized capillary tubes to gently touch the inner canthus, collecting approximately 300–400 μL of blood per mouse. The blood was immediately transferred to a pre-cooled EP tube, incubated at 4°C for 1 hour to allow clotting and contraction, then centrifuged at 4°C (3000 ×g, 15 minutes). The supernatant was aspirated and aliquoted into labeled EP tubes, then frozen at −80°C.

Statistical Analysis

All quantitative data are presented as Mean ± Standard Deviation (SD). Statistical analyses were performed using GraphPad Prism 8.0 software (GraphPad Software, Inc., USA). Differences between two groups were analyzed using the unrelated Student's *t*-test, while comparisons among multiple groups were performed using one-way Analysis of Variance (ANOVA) followed by Tukey's post-hoc test for multiple comparisons. A p-value of less than 0.05 ($p < 0.05$) was considered statistically significant.

Results and Discussion

Design and Manufacture of Biosensors

In this study, we present a novel biosensor based on a screen-printed electrode modified with a chemically responsive nanocoating. This sensor can selectively interact with tyrosinase, an enzyme biomarker in serum, and enables the early diagnosis of melanoma through enzyme-sensor electrochemical signal transduction (Figure 1). Specifically, we designed tyramine-functionalized multi-walled carbon nanotubes (MWCNTs) to establish selective recognition via the specific reaction between tyrosinase and tyramine, thereby developing a tool for the selective and sensitive detection of tyrosinase.[23,24] Carboxyl-functionalized MWCNTs (MWCNT-COOH) possess high catalytic activity, low reaction onset potential, large specific surface area, and can be modified through amide coupling and non-covalent π-π stacking. In this study, tyramine was covalently modified onto MWCNT-COOH via an amide reaction to obtain MWCNTs-tyr. Transmission electron microscopy (TEM) studies revealed no significant morphological differences between unmodified MWCNT-COOH and tyramine-modified MWCNT-COOH (Figure 2a and b). However, the introduction of tyramine

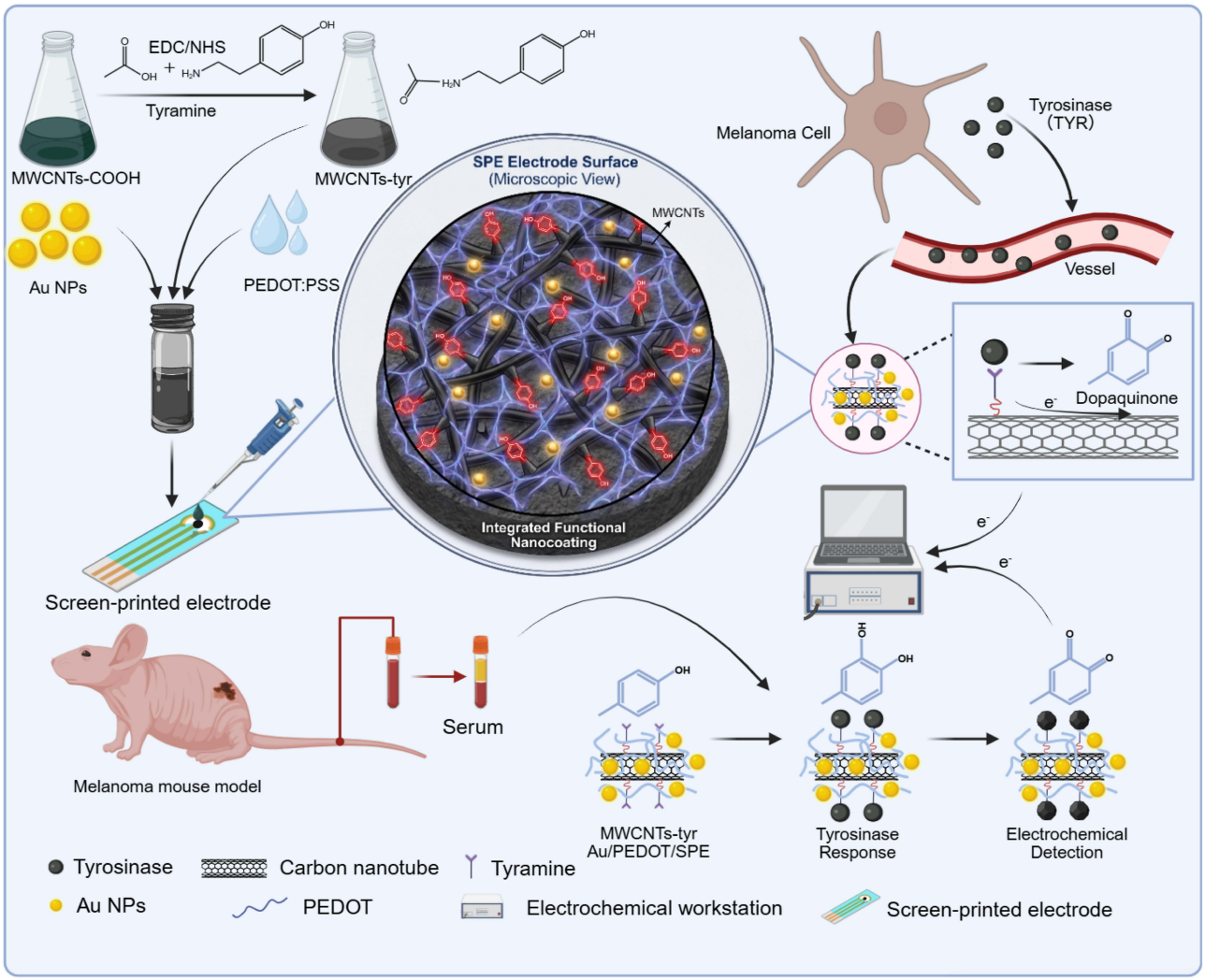

Figure 1 Schematic of an enzyme-responsive, activation-coated, screen-printed electrode for melanoma diagnosis. Enzyme-responsive, activation-type biosensor for detecting tyrosinase levels in tumor-bearing nude mouse serum (center); preparation process of the biosensor (top left); schematic of melanoma cells secreting tyrosinase into the bloodstream (top right); Collection of serum samples from melanoma-bearing mice (bottom left); Working principle of the biosensor (bottom right).

further improved the dispersibility of MWCNTs in water (Figure 2c), because the modification of the phenolic group enhanced the redox properties and dispersibility of MWCNTs-COOH.[25] Fourier transform infrared (FTIR) analysis showed that MWCNTs-tyr exhibited a new peak at 1634 cm^{-1}, which was attributed to the stretching vibration of C=O in the amide bond. Meanwhile, the stretching vibration of the phenolic hydroxyl group of tyramine and the N-H of the amide bond was enhanced at 3347 cm^{-1}, indicating the successful synthesis of MWCNTs-tyr (Figure 2d).

Decoration of metal nanoparticles (NPs) on multi-walled carbon nanotubes (MWCNTs) has been proven to enhance the conductivity of electrochemical sensors, and sensors prepared by this strategy have shown applications as sensors with high sensitivity and repeatability.[26] In this study, we used Au NPs and MWCNTs-tyr composites to improve the sensitivity and repeatability of the sensor. The attachment of Au NPs on the surface of MWCNTs was confirmed by transmission electron microscopy (TEM) (Figure 3a and b). Au NPs were randomly dispersed on the surface of MWCNTs in a spherical shape. The average diameter of MWCNTs determined from TEM micrographs was 20 ± 5 nm, while the average diameter of Au NPs was 50 ± 5 nm (Figure S1-2). The morphological and elemental characteristics of MWCNTs-tyr/Au were further examined using elemental mapping on high-angle annular dark-field scanning TEM (HAADF-STEM) (Figure 3c). The prepared MWCNTs-tyr/Au showed clear elemental signals of C, Au, and

https://doi.org/10.2147/IJN.S565641

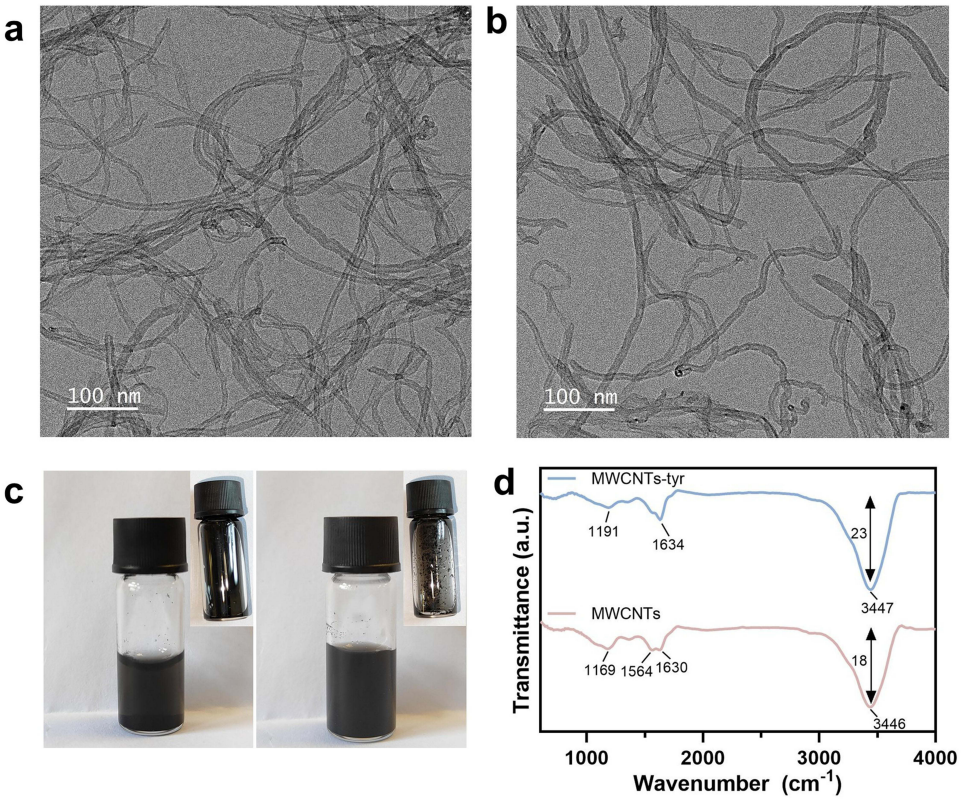

Figure 2 Material characterization of modified MWCNTs-COOH. (**a**) TEM image of MWCNTs-COOH; (**b**) TEM image of MWCNTs-tyr; (**c**) Dispersibility of MWCNTs-COOH (left) and MWCNTs-tyr (right); (**d**) FTIR spectra of MWCNTs-COOH and MWCNTs-tyr.

N from tyramine, which were also confirmed by recording their energy dispersive spectra, indicating the successful preparation of multi-walled carbon nanotubes loaded with Au NPs and tyramine (MWCNTs-tyr/Au).

Tyramine is a naturally occurring compound and a key substrate for tyrosinase.[27] To verify the effective loading of tyramine and AuNPs onto MWCNTs-COOH, the ultraviolet-visible (UV-Vis) absorption spectra of pure MWCNTs-COOH, AuNPs, MWCNTs-tyr, and MWCNTs-tyr/Au are presented in Figure 4. Tyramine, a decarboxylation product of tyrosine, features a phenol group in its core structure and typically exhibits a maximum UV absorption peak in the range of 275–282 nm.[28] After loading tyramine onto MWCNTs-COOH, the absorption peak appears at 262 nm, which is a shift of approximately 13–20 nm compared to that of free tyramine monomers. This shift may be attributed to the formation of a conjugated extended system or a charge transfer complex (CTC) between MWCNTs and tyramine.[29,30] The slight change in zeta potential between MWCNTs-COOH and MWCNTs-tyr also supports the successful modification with tyramine (Figure S3). In addition, after loading with AuNPs, MWCNTs-tyr shows the characteristic UV absorption peak of AuNPs at 542 nm, while the characteristic peak of tyramine at 262 nm does not weaken, indicating that the introduction of AuNPs does not affect the conformational stability of tyramine.

Surface Modification of SPE

In this work, two immobilization strategies were employed, namely non-covalent polymer matrix embedding and covalent modification via NHS/EDC. The non-covalent modification of the electrode was achieved by embedding MWCNTs-tyr/Au into the PEDOT:PSS structure. PEDOT:PSS is commonly used in the design of wearable biosensors due to its low cost, ease of processing, and biocompatibility.[31] Therefore, we used PEDOT:PSS combined with MWCNTs-tyr/Au as a composite mixture to fabricate the biosensor. PEDOT served as a stable conductive polymer matrix that not only entrapped the nanomaterials but also facilitated efficient electron transfer (Figure 5a). Scanning electron microscopy (SEM) revealed differences between the bare SPE electrode and the SPE electrode modified with MWCNTs-tyr/Au/PEDOT (Figure S4-5). A thin film was observed to cover the surface of the carbon nanotubes, indicating the successful modification of the electrode (Figure 5b). Elemental

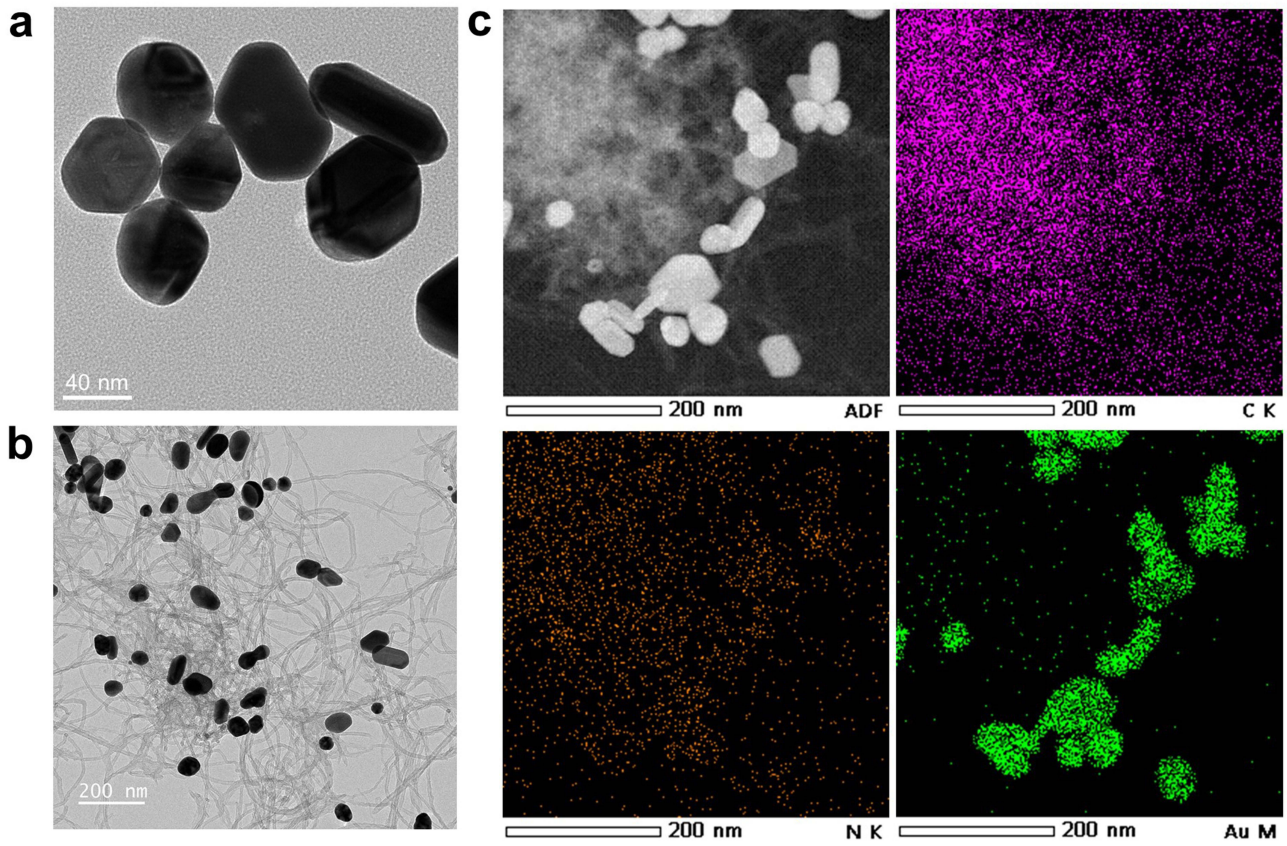

Figure 3 Materials characterization of MWCNTs-tyr/Au. (**a**) TEM image of Au nanoparticles. (**b**) TEM image of MWCNTs-tyr/Au composite material. (**c**) STEM image of MWCNTs-tyr/Au composite material.

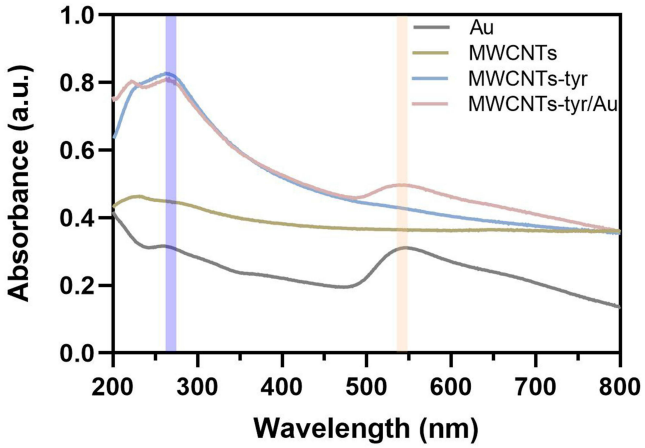

Figure 4 UV curves of AuNPs, MWCNTs, MWCNTs-tyr, AuNPs, and MWCNTs-tyr/Au.

analysis of the electrode surface using SEM mapping showed that elements such as C, N, Au, and S were uniformly distributed on the electrode (Figure 5c and S6). Meanwhile, the EDS spectrum indicated that the N element accounted for approximately 6.89% of the total elements, which collectively confirmed the successful fabrication of the SPE electrode loaded with tyramine (Figure S7). Coating uniformity: Although thickness is difficult to measure directly on rough SPE surfaces, we characterized coating uniformity and thickness via AFM (Figure 5d and e). Compared to the SPE electrode surface (Ra=53.3 nm, Rq=70.1 nm, Rmax=707 nm), the MWCNTs-tyr/Au/PEDOT-modified SPE electrode exhibited higher overall roughness (Ra=64.9 nm,

https://doi.org/10.2147/IJN.S565641

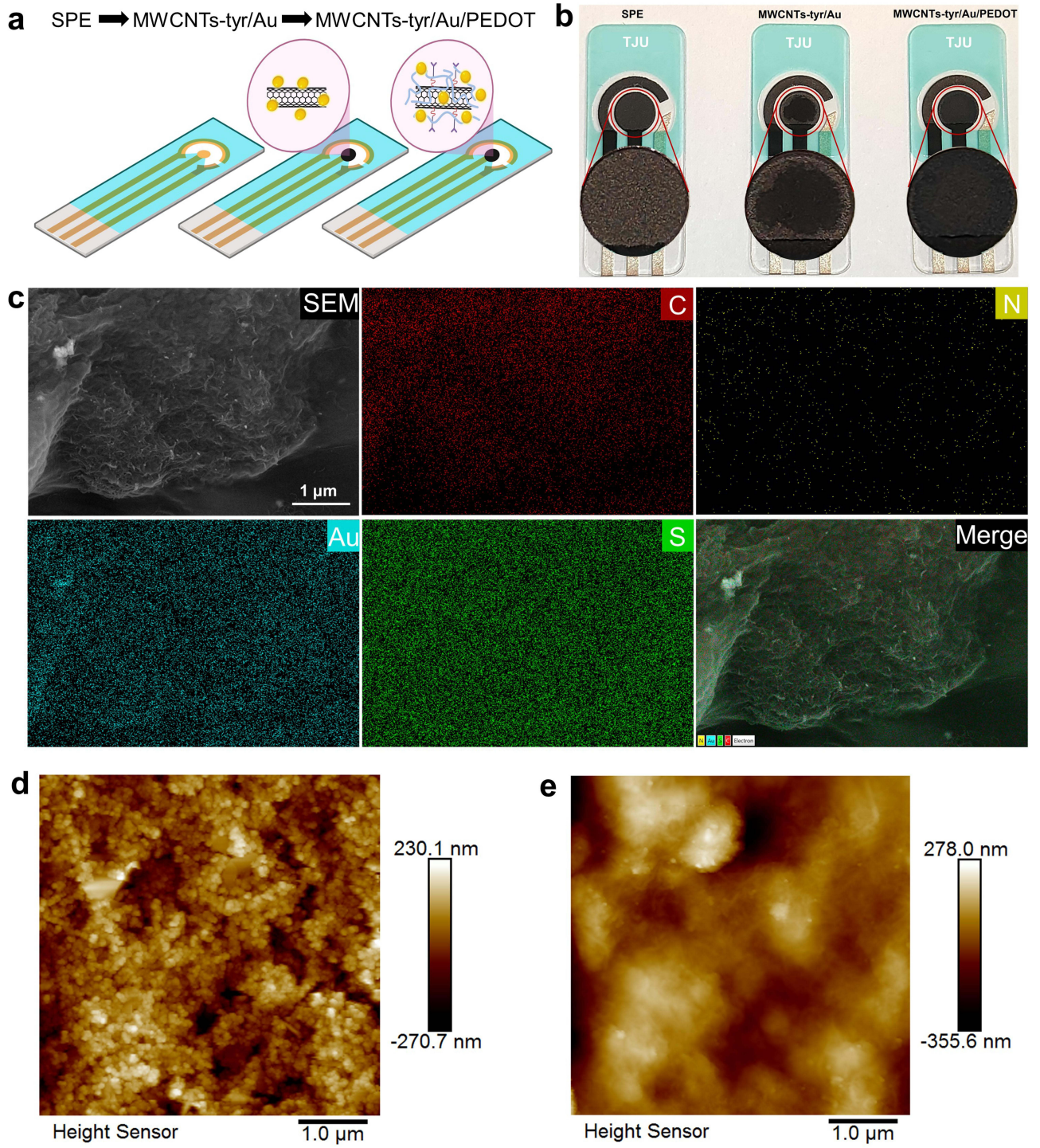

Figure 5 Modification and characterization of the SPE electrode. (**a**) Schematic diagram of the modified SPE electrode. (**b**) Physical image of the modified SPE electrode. In the enlarged view, it can be observed that MWCNTs-tyr/Au/PEDOT exhibits a more uniform distribution compared to MWCNTs-tyr/Au. (**c**) SEM image, elemental (C with red, N with yellow, Au with blue and S with green) mapping images and its merge image of the MWCNTS-ty/Au/PEDOT/SPE surface. (**d** and **e**) Characterization of SPE electrode (**d**) and MWCNTs-tyr/Au/PEDOT (**e**) Surface morphology and roughness using atomic force microscopy.

Rq=83.5 nm) but reduced local elevation variation (Rmax=588 nm). The results indicate that the modified electrode exhibits a more uniform height distribution, reducing mass transfer resistance and facilitating the diffusion of tyrosinase to the active centers and electrocatalytic sites on the electrode surface. Unlike the dense and complex microstructure of the pristine

electrode, the modified electrode demonstrates enhanced anti-fouling capability, promoting the timely diffusion and removal of tyrosinase after incubation. This improves electrode stability and reproducibility.

Electrochemical Study of Prepared MWCNTs-Tyr/Au/PEDOT/SPE Electrodes

Cyclic voltammetry (CV) and electrochemical impedance spectroscopy (EIS) were employed to analyze the electrochemical behaviors of biosensors with different modifications. Figure 6a shows the redox separation peaks of CV curves obtained at the SPE and MWCNTs-tyr/Au/PEDOT/SPE in a solution containing 5 mM $[Fe(CN)_6]^{3-/4-}$ with 0.1 M KCl at a fixed scan rate of 100 mV/s. Compared with the bare SPE, after modifying the SPE surface with MWCNTs-tyr/Au/PEDOT, the cathodic and anodic peak currents changed significantly, which remarkably reduced the difficulty of charge transfer between the electrode surface and the $[Fe(CN)_6]^{3-/4-}$ solution. Figure 6b and c present the Nyquist plots of the SPE electrode and MWCNTs-tyr/Au/PEDOT/SPE. The results indicate that conformational changes occurred on the electrode surface, the conductivity of the modified layer increased, and its resistance decreased. The slope of the straight line was 1.319 (close to 1), suggesting that the diffusion process was more consistent with the ideal Warburg behavior.[32] This demonstrates that MWCNTs-tyr/Au/PEDOT has been successfully immobilized on the SPE electrode, which significantly reduces the diffusion resistance on the electrode surface and is beneficial to improving the electrochemical reaction rate as well as the migration ability of ions and electrons.

The electron transfer behavior of the redox couple on the MWCNTs-tyr/Au/PEDOT/SPE electrode was investigated using CV measurements at different scan rates ranging from 50 to 300 mV s^{-1} in a 5 mM $[Fe(CN)_6]^{3-/4-}$ solution containing 0.1 M KCl (pH = 7.0). The results showed that the redox peak currents (Ip) (anodic (Ipa) and cathodic (Ipc) peaks) increased with the increasing scan rate of the electrode (Figure 6d). At 100 mV s^{-1}, the ratio of the peak currents of the anode (Ipa) to the cathode (Ipc) was approximately 1, indicating good redox quasi-reversibility of the MWCNTs-tyr/Au/PEDOT/SPCE electrode. Meanwhile, with the increase of scan rate, the positive shift of potential in the anodic peak current (Ipa) and the negative shift of potential in the cathodic peak current (Ipc) led to an increase in the peak separation potential (ΔE) value, further confirming the quasi-reversible process occurring on the electrode surface. Therefore, the fabrication of the MWCNTs-tyr/Au/PEDOT/SPE electrode was completely successful.

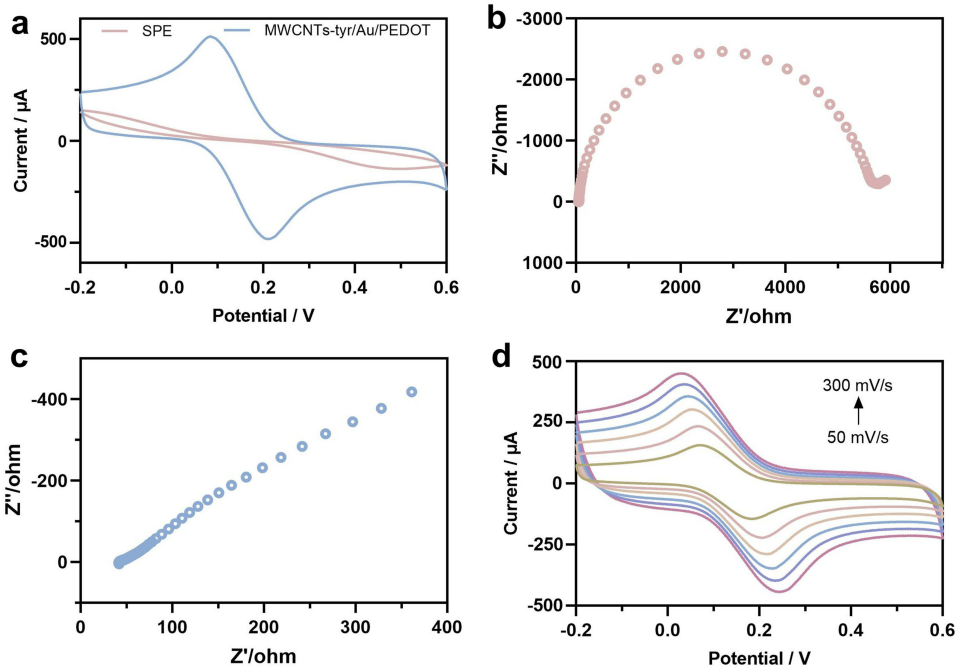

Figure 6 Electrochemical study of the prepared MWCNTs-tyr/Au/PEDOT/SPE electrode. (**a**) Cyclic voltammetry of the SPE and MWCNTs-tyr/Au/PEDOT/SPE electrodes under conditions containing 5 mM $[Fe(CN)_6]^{3-/4-}$ and 0.1 M KCl. (**b** and **c**) EIS curves of (**b**) SPE and (**c**) MWCNTs-tyr/Au/PEDOT electrode under conditions containing 5 mM $[Fe(CN)_6]^{3-/4-}$ indicator solution and 0.1 M KCl. (**d**) CV analysis of the MWCNTs-tyr/Au/PEDOT electrode at different scan rates.

https://doi.org/10.2147/IJN.S565641

Analytical Performance of MWCNTs-Tyr/Au/PEDOT for Tyrosinase

The electrochemical behaviors of MWCNTs-tyr/Au/PEDOT, tyrosinase, and their enzyme-catalyzed activation reactions were investigated by differential pulse voltammetry (DPV). Specifically, the MWCNTs-tyr/Au/PEDOT/SPE electrode was incubated with 0.4 U/L tyrosinase for 30 min (Figure 7a). Figure 7b displays the DPV curves of tyrosinase and its enzyme-catalyzed reaction in phosphate buffer solution (pH 7.0) within the potential range of −0.2 to 0.2 V, both before and after the modification of the SPE electrode. Evidently, for the bare SPE electrode, no oxidation peak was observed in PBS solution within this potential range regardless of the presence of tyrosinase. In contrast, the mixed solution of the MWCNTs-tyr/Au/PEDOT-modified SPE electrode after incubation with tyrosinase at room temperature for 30 min showed a clear oxidation peak (Ep = 0.0 V). The electrochemical signal transduction is governed by a "substrate-integrated" enzymatic activation mechanism, definitively validated by LC-MS analysis. The sensor surface is functionalized with tyramine. Upon exposure to the sample, serum tyrosinase catalyzes the specific ortho-hydroxylation of the surface-bound tyramine. As evidenced by the LC-MS results (Figure 7c and S8), this reaction successfully converts tyramine into dopamine (m/z 154.0865). The enzymatically generated dopamine possesses a redox-active catechol structure. Under the applied potential in DPV, dopamine undergoes a two-electron, two-proton oxidation to form dopamine-quinone (m/z 152.0709) (Figure 7d and S9). This electron transfer process generates a distinct anodic current peak. Since the amount of generated dopamine is directly proportional to the enzymatic activity of tyrosinase in the sample, the magnitude of the oxidation current serves as a precise quantitative measure of the tyrosinase concentration. The conductive MWCNTs/Au/PEDOT network further amplifies this electron flow, enabling the detection of ultralow biomarker levels. The results obtained from the DPV curves confirmed that tyrosinase can catalyze the oxidation of tyramine to form dopamine, and dopamine can be selectively and efficiently detected by these electrochemical methods.

Differential pulse voltammetry (DPV) was employed to investigate the response of the MWCNTs-tyr/Au/PEDOT/SPE electrode to increasing concentrations of tyrosinase (TYR) (0.05–0.9 U/L) in phosphate buffer solution (PBS) at pH 7.0, with a scan rate of 100 mV s^{-1}. The results are presented in Figure 7e. The DPV curves reveal that the MWCNTs-tyr/Au/PEDOT/SPE biosensor exhibits a continuously increasing current response across the entire concentration range. Specifically, the current value rises with the increase in TYR concentration, demonstrating excellent performance of the sensor for tyrosinase detection. Meanwhile, a graph plotting the peak current (μA) against TYR concentration (U/L) was constructed. From this graph, it can be observed that the MWCNTs-tyr/Au/PEDOT/SPE electrode has a single linear region (Figure 7f). The sensor shows a linear response to tyrosinase as low as 0.05 U/L (regression coefficient (R^2) = 0.9914). Based on the slope, a sensitivity of 20.27 μA $U^{-1}L^{-1}$ was calculated. Additionally, the limit of detection was determined to be 0.0091 U/L at a signal-to-noise ratio (S/N) of 3. The superior sensing performance is attributed to the strong electron transfer capability and enzymatic efficiency of the MWCNTs-tyr/Au/PEDOT/SPE. The calibration sensitivity (slope) in diluted serum was 96.1% of that in PBS (Figure S10), indicating that the PEDOT/Au coating effectively minimizes biofouling and matrix interference. Spike-and-recovery tests in serum samples yielded recoveries ranging from 96.0% to 103.7%, confirming the sensor's accuracy in complex biological matrices (Table S1).

Stability and Interference Resistance Testing

Meanwhile, to determine the repeatability and stability of the MWCNTs-tyr/Au/PEDOT/SPE electrode, independent experiments were repeated using the same electrode or different electrodes with 0.1 U/L and 0.9 U/L tyrosinase (TYR). Among them, the same electrode could be used for repeated measurements five times at a tyrosinase concentration of 0.1 U/L, indicating good reproducibility of the electrode (Figure 8a). However, when the concentration was increased to 0.9 U/L, the current signal decreased and eventually disappeared after the third measurement, which was due to the complete occupation and oxidation of all monophenol sites on the MWCNTs-tyr/Au/PEDOT/SPE electrode to quinones. Furthermore, we evaluated the stability of different MWCNTs-tyr/Au/PEDOT/SPE electrodes. Results indicate that the performance of all electrodes remained relatively stable in the presence of 0.1 U/L and 0.9 U/L tyrosine, with no significant differences observed (Figure 8b). After 4 weeks, the sensors still maintained >90% of their initial response values. In addition, the specificity or anti-interference performance of MWCNTs-tyr/Au/PEDOT/SPE was also evaluated. Due to the particularity of the MWCNTs-tyr/Au/PEDOT/SPE electrode, it can only be activated by the specific catalytic action of tyrosinase. We incubated

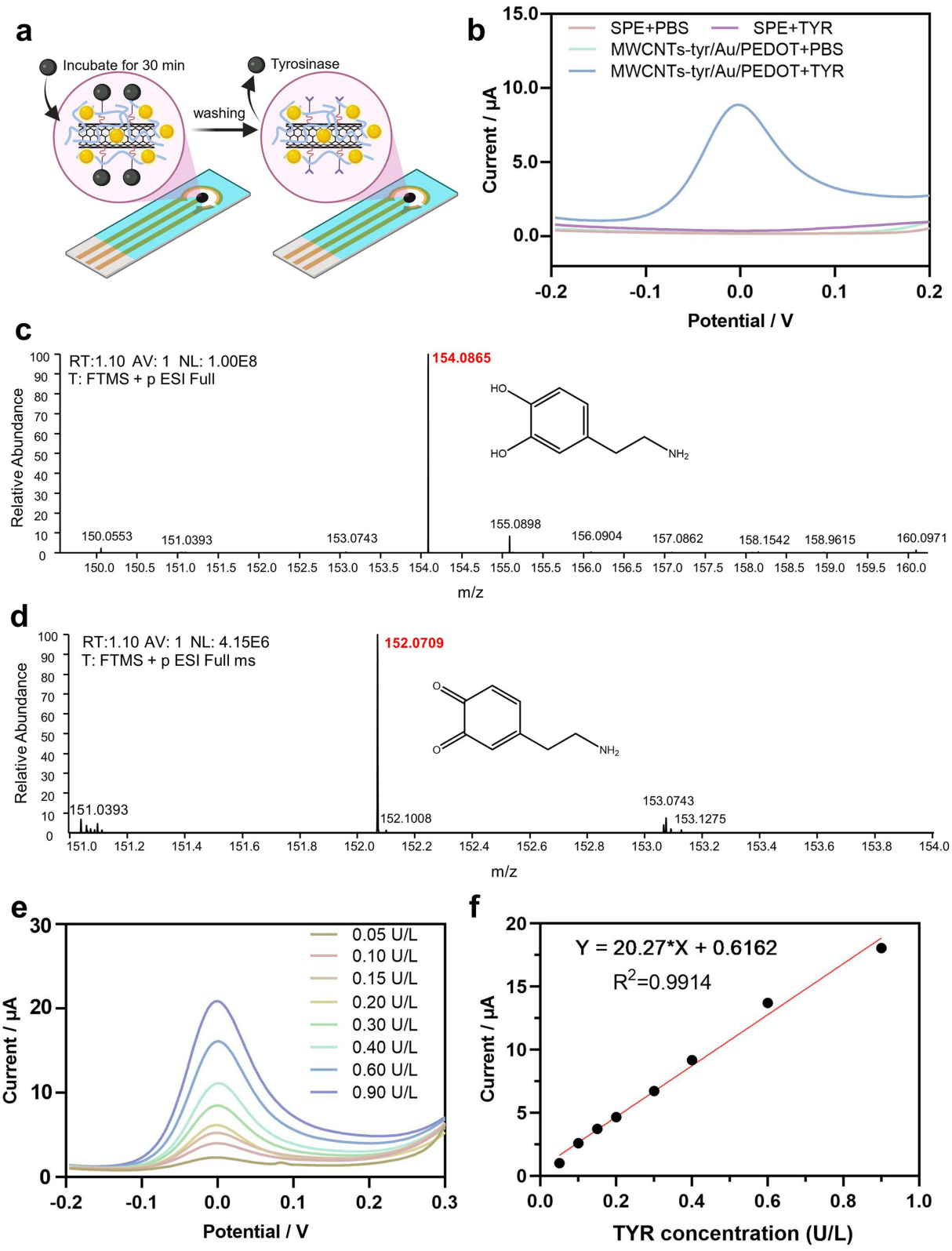

Figure 7 Current responses of the electrode to different concentrations of tyrosinase (TYR) via DPV. (**a**) Schematic illustration of MWCNTs-tyr/Au/PEDOT/SPE for tyrosinase detection. (**b**) Responsiveness of SPE and MWCNTs-tyr/Au/PEDOT/SPE to tyrosinase. (**c** and **d**) Full scan MS^1 spectrum of dopamine (**c**) and dopamine-quinone (**d**) in positive electrospray ionization (ESI^+) mode, showing the protonated molecular ion $[M+H]^+$ at m/z 152.07 and the chemical structure. (**e**) DPV current responses of the MWCNTs-tyr/Au/PEDOT/SPE electrode at low tyrosinase concentrations (0.05–0.90 U/L). (**f**) Linear relationship between tyrosinase concentration and current.

https://doi.org/10.2147/IJN.S565641

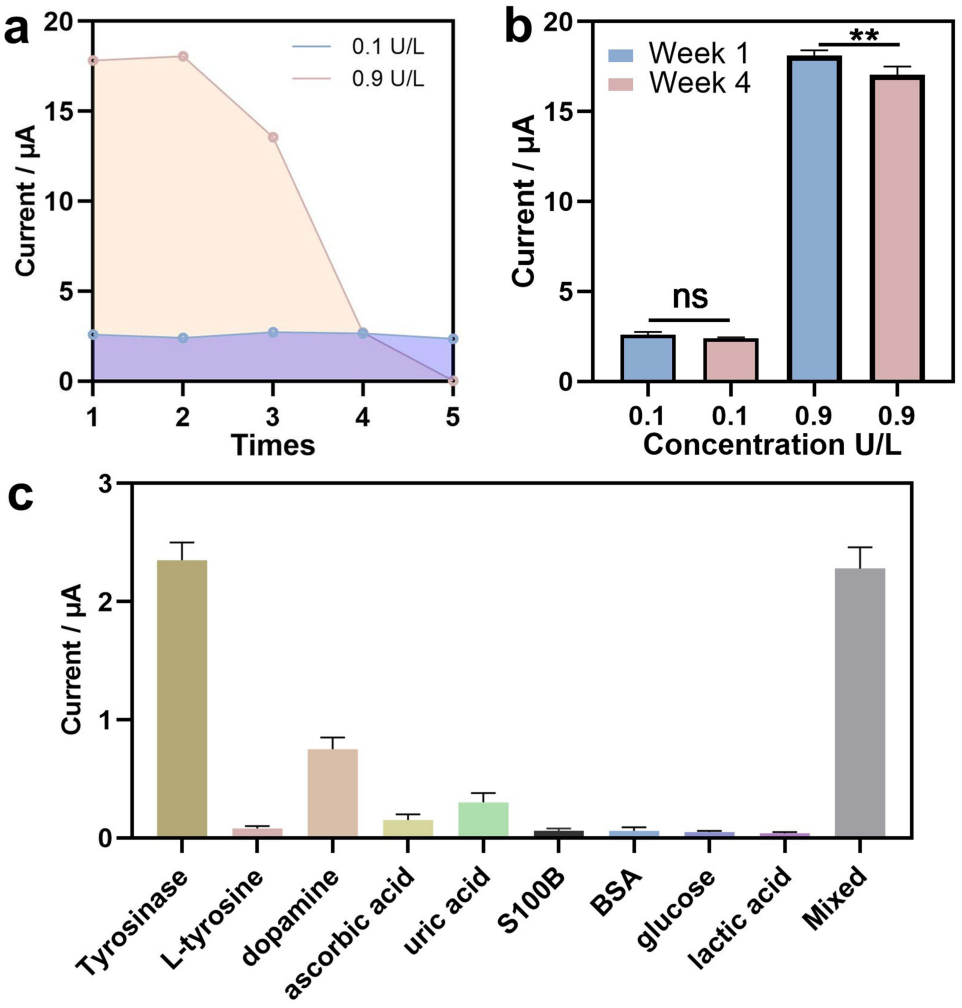

Figure 8 Stability and anti-interference performance of the MWCNTs-tyr/Au/PEDOT/SPE electrode. (**a**) Current signal attenuation when measuring 0.1 U/mL and 0.9 U/mL tyrosinase continuously for five times using the same electrode. (**b**) Measure the current signal repeatability at 0.1 U/mL and 0.9 U/mL tyrosinase using different electrodes during Week 1 and Week 4. (**c**) Current responses of the MWCNTs-tyr/Au/PEDOT/SPE electrode for the detection of 10 μM L-tyrosine, 10 μM dopamine, 10 μM ascorbic acid, 10 μM uric acid, 1 mg/L S100B protein. 10 g/L BSA protein, 1 mM glucose, and 50 μM lactic acid. n=5, data are expressed as mean ± standard deviation (SD), *$p < 0.05$, **$p < 0.01$, ns (not significant, $p > 0.05$).

the MWCNTs-tyr/Au/PEDOT/SPE sensor with common interfering substances in serum, and eluted the test substances after 30 min. The results showed that a significant signal response could only be induced by tyrosinase, while other control samples could not induce any significant signal response. Moreover, the combined addition of tyrosinase and interfering substances did not affect the signal of the MWCNTs-tyr/Au/PEDOT/SPE sensor (Figure 8c). This excellent specificity can be attributed to the adopted enzyme-catalyzed activation electrochemical sensing mechanism. Without tyrosinase pretreatment, interfering substances cannot trigger the conversion of monophenols to polyphenols in the sensor, which also ensures better anti-interference effect for direct detection of clinical serum samples without any pretreatment.

Graded Evaluation of Mouse Melanoma Using MWCNTs-Tyr/Au/PEDOT/SPE Electrode Biosensors

As mentioned above, the developed MWCNTs-tyr/Au/PEDOT/SPE platform exhibits excellent selectivity and sensitivity. Tyrosinase has been proven to be an important biomarker for melanoma, providing a useful platform for the detection of tyrosinase in biological systems. Therefore, we employed the current MWCNTs-tyr/Au/PEDOT/SPE to detect tyrosinase activity in the serum of tumor-bearing mice. We subcutaneously inoculated nude mice with B16/F10 cells. Subsequently, the serum of tumor-bearing mice was collected on days 0, 4, 8, and 12 after tumor induction, and tyrosinase signals were

detected at three key time windows after tumor implantation (Figure 9a and b, S11). With the increase of tumor volume (68n ± 5.25 mm^3, 494 ± 26.72 mm^3, 1280 ± 89.22 mm^3), the concentration of tyrosinase in serum also increased, which were 0.084 ± 0.009 U/L, 0.169 ± 0.011 U/L, and 0.653 ± 0.028 U/L, respectively (Figure 9c–e, S12). Furthermore, we tested actual samples using ELISA experiments. As shown in Figures 9f and S13-14, the biosensor readings exhibited strong linear correlation with ELISA detection values (R^2 = 0.9926), confirming the accuracy of this method. To validate that the enhanced tyrosinase signal specifically originates from melanoma rather than systemic tumor burden artifacts, we conducted supplementary experiments using the 4T1 tumor model. Serum samples were collected when tumor volume reached levels comparable to the melanoma group (approximately 1200 mm^3). As shown in Figure 9g, the 4T1 tumor group exhibited a faint signal response (0.015 ± 0.005 U/L), showing no statistically significant difference compared to the healthy baseline. These results demonstrate that the biosensor possesses a strong ability to distinguish between different stages of melanoma, highlighting its potential clinical application value in melanoma diagnosis.

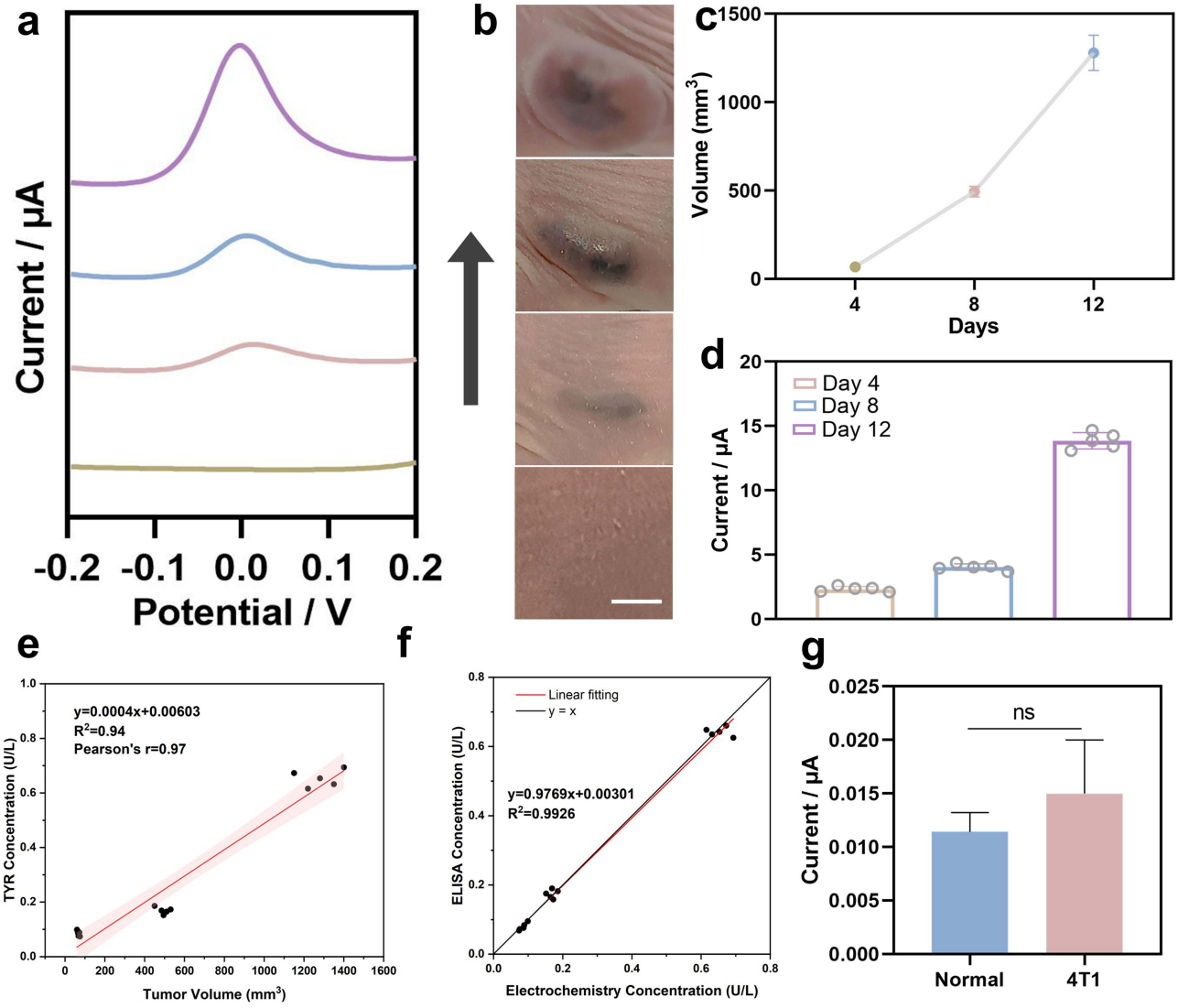

Figure 9 MWCNTs-tyr/Au/PEDOT/SPE for real sample detection. (**a**) DPV response of tyrosinase in the serum of tumor-bearing mice. (**b**) Growth status of cutaneous melanoma in tumor-bearing mice and (**c**) growth curve, Scale bar: 500 μm. (**d**) Statistical values of current responses of MWCNTs-tyr/Au/PEDOT/SPE to tyrosinase in the serum of tumor-bearing mice. (**e**) A statistical analysis was conducted to examine the correlation between tumor volume and serum tyrosinase concentration. (**f**) Comparison of Linear Correlation Between MWCNTs-tyr/Au/PEDOT/SPE Biosensor and TYR ELISA Kit. (**g**) Statistical values of the current responses of MWCNTs-tyr/Au/PEDOT/SPE to tyrosinase in serum from normal mice and 4T1 tumor-bearing mice. n=5, data are expressed as mean ± standard deviation (SD), ns (not significant, $p > 0.05$).

https://doi.org/10.2147/IJN.S565641

Discussion

The development of electrochemical biosensors for specific biomarker detection requires meticulous design of the sensing interface to achieve high sensitivity and selectivity.[33,34] This is particularly critical for early melanoma diagnosis, where biomarker levels are low and sample matrices are complex.[35] This study designed and fabricated a novel electrochemical biosensor centered on a tyramine-modified multi-walled carbon nanotube-gold nanoparticle composite (MWCNTs-tyr/Au). This composite was integrated into a poly (ethylene glycol) monosodium (styrene sulfonate) copolymer (PEDOT: PSS) matrix on a screen-printed carbon electrode (SPCE) for the specific detection of the enzymatic biomarker tyrosinase (TYR).

The fundamental mechanism relies on the difference in redox behavior between the substrate and the product. The immobilized tyramine is electrochemically inert within the low potential window used. Upon exposure to the sample, tyrosinase catalyzes the ortho-hydroxylation of the phenol ring, converting tyramine into dopamine. Unlike tyramine, dopamine possesses a catechol structure, which is a well-known redox-active moiety. Under the applied DPV potential, the generated surface-bound dopamine undergoes a reversible two-electron, two-proton ($2e^-/2H^+$) oxidation process to form dopamine-quinone (Equation 1)

$$Dopamine \leftrightharpoons Dopamine - quinone + 2H^+ + 2e^-$$

This oxidation event releases electrons to the electrode, generating the measurable anodic current. The magnitude of this current is directly proportional to the surface concentration of dopamine, which in turn correlates with the enzymatic activity of TYR in the serum.

Strategic functionalization of nanomaterials forms the foundation of biosensor design, determining the platform's recognition capabilities and electrochemical properties.[36,37] The core design of this biosensor relies on the specific enzymatic reaction between TYR and its substrate tyramine.[38] Functionalization of MWCNT-COOH with tyramine was confirmed via Fourier Transform Infrared Spectroscopy (FTIR), revealing characteristic peaks corresponding to amide bonds. The incorporation of tyramine not only provides specific recognition sites but also enhances MWCNT dispersion in aqueous solutions, facilitating subsequent processing and electrode modification. Furthermore, TEM, HAADF-STEM elemental mapping, and UV-Vis spectroscopy confirmed that gold nanoparticle modification significantly enhanced the nanocomposite's electrical conductivity and catalytic activity. The shift in the UV absorption peak after tyramine conjugation with MWCNTs indicates the formation of an extended conjugated system or charge-transfer complex, potentially contributing to improved electron transfer efficiency.

To translate the properties of nanocomposites into reliable electrode interfaces, stable and efficient immobilization strategies are crucial.[39,40] The nanocomposite was stabilized on the SPCE surface via embedding within PEDOT: PSS. SEM imaging and elemental mapping confirmed the uniform distribution of C, N, Au, and S elements within the modified layer, indicating successful electrode preparation. Cyclic voltammetry (CV) and electrochemical impedance spectroscopy (EIS) characterization revealed that the MWCNTs-tyr/Au/PEDOT modified layer significantly enhanced charge transfer kinetics at the electrode-solution interface while reducing diffusion resistance. The Warburg effect and quasi-reversible electron transfer processes further confirmed the promoting effect of this modified layer on electrochemical reactions.

Analytical validation of biosensors under controlled conditions is a prerequisite for assessing their practical application potential.[41] The analytical performance of this sensor was evaluated using DPV, a distinct oxidation peak was observed only at 0.0 V after incubation with tyramine, confirming the electrochemical detectability of the enzymatic oxidation of tyramine to dopamine. The sensor exhibited a broad linear response range (0.05–0.9 U/L), high sensitivity (20.27 μA U-1 L-1), and a low detection limit (0.0091 U/L) with quantitation limit (0.0303 U/L). Excellent reproducibility and stability at lower tyramine concentrations (0.1 U/L), coupled with minimal interference from common serum biomolecules, highlight the robustness and specificity of this sensing mechanism. Signal attenuation observed after multiple measurements at 0.9 U/L tyramine concentration is attributed to saturation and irreversible oxidation of the phenolic hydroxyl site, indicating limited applicability for repeated measurements under high-concentration conditions. Therefore, this sensor is defined as a single-use device to ensure maximum accuracy, rather than a reusable probe. The ultimate value of biosensors lies in their ability to reliably detect biomarkers in clinically relevant samples. Most

importantly, the practical utility of this biosensor in biological scenarios was validated through successful monitoring of tyrosinase activity in serum samples from a mouse melanoma model. Elevated tyrosinase levels correlate positively with tumor progression, highlighting the platform's potential for non-invasive early diagnosis and staging of melanoma.

Conclusions

In this work, we successfully fabricated a disposable electrochemical biosensor based on a MWCNTs-tyr/Au/PEDOT nanocomposite for the sensitive detection of tyrosinase (TYR). The sensor demonstrated superior analytical performance, achieving a low detection limit of 0.0091 U/L and a wide linear range of 0.05–0.9 U/L, which effectively addresses the sensitivity limitations and anti-interference challenges of conventional detection methods. In vivo experiments in a tumor-bearing mouse model validated the biological applicability of the sensor, revealing a significant positive correlation between serum TYR levels and tumor volume (from 0.084 U/L to 0.653 U/L as tumors progressed). These findings confirm the sensor's capability for staging discrimination in animal models and establish it as a promising preclinical tool for the early screening and longitudinal monitoring of melanoma. Future work will focus on validating this platform in human clinical cohorts to further assess its translational potential.

Data Sharing Statement

All data are available in the main text or the supplementary information.

Ethics Approval and Informed Consent

All animal procedures were performed in strict accordance with the Guide for the Care and Use of Laboratory Animals (8th edition, National Institutes of Health) and were approved by the Animal Ethics Committee of Tongji University (Approval No. TJAA09724101).

Author Contributions

All authors made a significant contribution to the work reported, whether that is in the conception, study design, execution, acquisition of data, analysis and interpretation, or in all these areas; took part in drafting, revising or critically reviewing the article; gave final approval of the version to be published; have agreed on the journal to which the article has been submitted; and agree to be accountable for all aspects of the work.

Funding

This work was supported by the East Hospital Affiliated to Tongji University Introduced Talent Research Startup Fund (Grant No. DFRC2019008), and the Featured Clinical Discipline Project of Shanghai East Hospital (Grant No. 2024-DFTS-007).

Disclosure

The authors declare no conflicts of interest in this work.

References

1. Li KH, Cheung PCF, Petrella TM, Zhang L, Poon IDT, Menjak IB. Clinical outcomes of multisite moderate to high dose radiotherapy for patients with metastatic melanoma. *Precision Radiat Oncol*. 2024;8(2):62–69. doi:10.1002/pro6.1224
2. Ding L, Gosh A, Lee DJ, et al. Prognostic biomarkers of cutaneous melanoma. *Photodermatol Photoimmunol Photomed*. 2022;38(5):418–434. doi:10.1111/phpp.12770
3. Peng H, Wang T, Li G, Huang J, Yuan Q. Dual-locked near-infrared fluorescent probes for precise detection of melanoma via hydrogen peroxide–tyrosinase cascade activation. *Anal Chem*. 2021;94(2):1070–1075. doi:10.1021/acs.analchem.1c04058
4. Nwafor NJ, Torere BE, Agu E, et al. The role of biomarkers in the diagnosis and prognosis of different stages of melanoma. *Cureus*. 2023;15(5): e38693. doi:10.7759/cureus.38693
5. Elmasry MR, Shaban SM, Abualrejal MMA, et al. Integrated colorimetric and fluorescent assay using gold nanobipyramids and UCNPs for tyrosinase-based melanoma diagnostics. *Biochip J*. 2025;19:198–806. doi:10.1007/s13206-025-00223-0
6. Sonesson B, Eide S, Rorsman H, et al. Tyrosinase activity in the serum of patients with malignant melanoma. *Melanoma Re*. 1995;5(2):113–116. doi:10.1097/00008390-199504000-00007

7. Tyurina YY, Kapralov AA, Tyurin VA, et al. Redox phospholipidomics discovers pro-ferroptotic death signals in A375 melanoma cells in vitro and in vivo. *Redox Biol*. 2023:61. doi:10.1016/j.redox.2023.102650.
8. Fauss D, Motter R, Dofiles L, et al. Development of an enzyme-linked immunosorbent assay (ELISA) to measure the level of tyrosine hydroxylase protein in brain tissue from Parkinson's disease models. *J Neurosci Meth*. 2013;215(2):245–257. doi:10.1016/j.jneumeth.2013.03.012
9. Singh A, Sharma A, Ahmed A, et al. Recent advances in electrochemical biosensors: applications, challenges, and future scope. *Biosensors*. 2021;11(9). doi:10.3390/bios11090336
10. Shi Z, Liu W, Liu X, et al. Magnetic separation-integrated electrochemical biosensor with synergy of photo-electronic cascading for high-reproducibility detection of miRNA biomarker in tumor tissue. *Talanta*. 2026:297. doi:10.1016/j.talanta.2025.128675.
11. He C, Liu H, Yin M, et al. A UOx@HMnO 2 biozyme–nanozyme driven electrochemical platform for specific uric acid bioassays. *Analyst*. 2025;150(7):1377–1385. doi:10.1039/d4an01512f
12. Chen X, Feng X-Z, Zhan T, et al. Construction of a portable enzyme-free electrochemical glucose detection system based on the synergistic interaction of Cu-MOF and PtNPs. *Sensors and Actuat B Chem*. 2023:395. doi:10.1016/j.snb.2023.134498.
13. Cheng -Y-Y, Feng X-Z, Zhan T, et al. A facile indole probe for ultrasensitive immunosensor fabrication toward C-reactive protein sensing. *Talanta*. 2023:262. doi:10.1016/j.talanta.2023.124696.
14. Tu W, Sun M, Lu T, et al. Wearable electrochemical aptasensor based on MXene@gold nanoparticles for non-invasive sweat cortisol detection. *Biosens Bioelectron*. 2025:287. doi:10.1016/j.bios.2025.117736.
15. Lee T-W, Park -H-H. The effect of MWCNTs on the electrical properties of a stretchable carbon composite electrode. *Compos Sci Technol*. 2015;114:11–16. doi:10.1016/j.compscitech.2015.03.020
16. Chen X, Wu C, Lv Y, et al. Highly active nitrogen-phosphorus co-doped carbon fiber@graphite felt electrode for high-performance vanadium redox flow battery. *J Colloid Interface Sci*. 2025;677:683–691. doi:10.1016/j.jcis.2024.08.091
17. Solomon EI, Sundaram UM, Machonkin TE. Multicopper oxidases and oxygenases. *Chem Rev*. 1995;96(7):2563–2606. doi:10.1021/cr950046o
18. Ramsden CA, Riley PA. Tyrosinase: the four oxidation states of the active site and their relevance to enzymatic activation, oxidation and inactivation. *Bioorg Med Chem*. 2014;22(8):2388–2395. doi:10.1016/j.bmc.2014.02.048
19. Tasis D, Tagmatarchis N, Bianco A, Prato M. Chemistry of carbon nanotubes. *Chem Rev*. 2006;106(3):1105–1136. doi:10.1021/cr050569o
20. Suherman AL, Kuss S, Tanner EEL, Young NP, Compton RG. Electrochemical Hg2+detection at tannic acid-gold nanoparticle modified electrodes by square wave voltammetry. *Analyst*. 2018;143(9):2035–2041. doi:10.1039/C8AN00508G
21. Chen Z, Meng X, Wang S, et al. PEDOT: PSS-MWCNTs modified carbon black-based gas diffusion electrodes for improved performance of in-situ electrocatalytic flue gas desulfurization. *J Cleaner Prod*. 2018;200:1087–1099. doi:10.1016/j.jclepro.2018.07.262
22. Pourahmadi E, Ganesan R, Shadmehri F. Micromechanical characterization of Carbon/PEEK thermoplastic composite material in-situ consolidated by automated fiber placement: stiffness prediction. *Compos Sci Technol*. 2024;246. doi:10.1016/j.compscitech.2023.110390
23. Kweon DH, Okyay MS, Kim S-J, et al. Ruthenium anchored on carbon nanotube electrocatalyst for hydrogen production with enhanced Faradaic efficiency. *Nat Commun*. 2020;11(1). doi:10.1038/s41467-020-15069-3
24. Tuttle MR, Davis S, Zhang S. Synergistic effect of hydrogen bonding and π-π stacking enables long cycle life in organic electrode materials. *ChemRxiv*. 2020. doi:10.26434/chemrxiv.13259303.v1
25. Tuci G, Bonechi M, Rossin A, et al. Mildly oxidized and phenol-enriched carbon nanotubes as efficient and selective electrocatalysts for the 2e$^-$oxygen reduction reaction. *Chem Synth*. 2025;5(4). doi:10.20517/cs.2025.05
26. Mehmood S, Ciancio R, Carlino E, Bhatti A. Role of Au(NPs) in the enhanced response of Au(NPs)-decorated MWCNT electrochemical biosensor. *Int J Nanomed*. 2018;13:2093–2106. doi:10.2147/IJN.S155388
27. Goldfeder M, Kanteev M, Isaschar-Ovdat S, Adir N, Fishman A. Determination of tyrosinase substrate-binding modes reveals mechanistic differences between type-3 copper proteins. *Nat Commun*. 2014;5(1). doi:10.1038/ncomms5505
28. Antosiewicz JM, Shugar D. UV-Vis spectroscopy of tyrosine side-groups in studies of protein structure. Part 1: basic principles and properties of tyrosine chromophore. *Biophys Rev*. 2016;8(2):151–161. doi:10.1007/s12551-016-0198-6
29. Mingchien C, Weixiao H. Investigation of Ct-complexation among homologous electron donors and homlogous acceptors II. geometrical match effect. *Acta Physico-Chimica Sinica*. 1987;3(03):298–305. doi:10.3866/PKU.WHXB19870314
30. Feng W, Yi WH, Feng YY, Wu ZG, Zhang ZZ. In-situ polymerization and third-order nonlinear optical properties of polyaniline/carbon natotube composite. *Acta Phys Sinica*. 2006;55(7). doi:10.7498/aps.55.3772
31. Yang P, Xiang S, Li R, et al. Highly stretchable and sensitive flexible strain sensor based on Fe NWs/Graphene/PEDOT:PSS with a porous structure. *Int J Mol Sci*. 2022;23(16). doi:10.3390/ijms23168895
32. Brett CMA. Electrochemical impedance spectroscopy in the characterisation and application of modified electrodes for electrochemical sensors and biosensors. *Molecules*. 2022;27(5):1497. doi:10.3390/molecules27051497
33. Turner APF. Biosensors: sense and sensibility. *Chem Soc Rev*. 2013;42(8):3184–96.
34. Justino CIL, Gomes AR, Freitas AC, Duarte AC, Rocha-Santos TAP. Graphene based sensors and biosensors. *TrAC Trends Anal Chem*. 2017;91:53–66. doi:10.1016/j.trac.2017.04.003
35. Merlino G, Herlyn M, Fisher DE, et al. The state of melanoma: challenges and opportunities. *Pigm Cell Mel Res*. 2016;29(4):404–416. doi:10.1111/pcmr.12475
36. Mostafa AM, Barton SJ, Wren SP, Barker J. Review on molecularly imprinted polymers with a focus on their application to the analysis of protein biomarkers. *TrAC Trends Anal Chem*. 2021;144. doi:10.1016/j.trac.2021.116431
37. Li L, Wang T, Zhong Y, et al. A review of nanomaterials for biosensing applications. *J Mater Chem B*. 2024;12:1168–1193. doi:10.1039/d3tb02648e
38. Deng M, Feng J, Tao D, et al. A novel conductive nanocomposite-based biosensor for ultrasensitive detection of microRNA-21 in serum, using methylene blue as mediator. *Bioelectrochemistry*. 2022;148:108256. doi:10.1016/j.bioelechem.2022.108256
39. Nashruddin S, Abdullah J, Mohammad HM, Mat ZM, Choon O, Mohd RWM. Label free glucose electrochemical biosensor based on Poly(3,4--ethylenedioxy thiophene): Polystyrene Sulfonate/Titanium Carbide/Graphene Quantum Dots. *Biosensors*. 2021;11(8):267. doi:10.3390/bios11080267
40. Zhu Y, Xu Z, Gao J, Ji W, Zhang J. An antibody-aptamer sandwich cathodic photoelectrochemical biosensor for the detection of progesterone. *Biosens Bioelectron*. 2020;160. doi:10.1016/j.bios.2020.112210
41. Kalaiyarasan G, Joseph J. Processes in biosensor design, development, and validation parameters. *Health Environ Appl Biosensing Technol*. 2024;27–49. doi:10.1016/B978-0-443-19039-1.00002-X